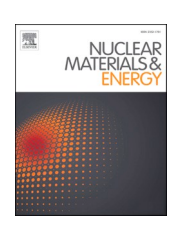
ELSEVIER

Contents lists available at ScienceDirect

Nuclear Materials and Energy

journal homepage: www.elsevier.com/locate/nme





Testing of ITER-grade plasma facing units in the WEST tokamak: Progress in understanding heat loading and damage mechanisms

- Y. Corre a,*, M-H. Aumeunier A. Durif J. Gaspar, K. Krieger, T. Loewenhoff, M. Richou,
- S. Ratynskaia^e, Q. Tichit^a, Y. Anquetin^b, R. Dejarnac^f, M. Diez^a, L. Dubus^a, M. Firdaouss^a,
- J. Gerardin^a, A.. Grosjean^a, J.P. Gunn^a, T. Loarer^a, P. Maget^a, C. Martin^g, K. Paschalidis^e,
- E. Tsitrone a, M. Wirtz d, 1, the WEST team
- ^a CEA, Institute for Research on Fusion by Magnetic confinement, 13108 St-Paul-Lez-Durance, France
- ^b Aix Marseille Univ, CNRS, IUSTI, Marseille, France
- ^c Max-Planck-Institut für Plasmaphysik, 85748 Garching b. München, Germany
- ^d Forschungszentrum Jülich GmbH, Institut für Energie und Klimaforschung, 52425 Jülich, Germany
- ^e Space and Plasma Physics, KTH Royal Institute of Technology, SE-10044, Stockholm, Sweden
- f Institute of Plasma Physics, Czech Academy of Sciences, 182 00 Prague, Czech Republic
- g Aix Marseille Univ, PIIM UMR 7345, F-13397 Marseille, France

ARTICLE INFO

Keywords: Tungsten cracking Melting Plasma Facing Unit Heat flux calculation IR thermography

ABSTRACT

Assessing the performance of the ITER design for the tungsten (W) divertor Plasma Facing Units (PFUs) in a tokamak environment is a high priority issue to ensure efficient plasma operation. This paper reviews the most recent results derived from experiments and post-mortem analysis of the ITER-grade PFUs exposed in the WEST tokamak and the associated modelling, with a focus on understanding heat loading and damage evolution. Several shaping options, sharp or chamfered leading edge (LE), unshaped or shaped blocks with a toroidal bevel as foreseen in ITER, were investigated, under steady state heat fluxes of up to $120 \, \mathrm{MW \, m^{-2}}$ and $6 \, \mathrm{MW \, m^{-2}}$ on the sharp LE and top surface of the block, respectively. A very high spatial resolution (VHR) infrared (IR) camera (0.1 mm/pixel) was used to derive the temporal and surface distribution of the temperature and heat load on the castellated tungsten blocks for different geometric alignment and plasma conditions. Photonic modelling was required to reproduce the IR measurements in particular in the toroidal and poloidal gaps of the mono-block (MB) stacks where high apparent temperatures are observed. Specular reflection is found to be the dominant emitter in these parts of the blocks. W-cracking was observed on the leading edge of the blocks already within the first phase of plasma operation, during which the divertor was equipped with unshaped PFUs, including some intentionally misaligned blocks. Numerical analysis taking into account softening processes and mechanical stresses, revealed brittle failure due to transients as the dominant failure mechanisms. Ductile failure was observed in one particular block used for the melting experiment, therefore under extremely high steady state heat load conditions. W-melting achieved on actively cooled PFU exhibits specific features: shallow melting and slow melt displacement. Plasma exposure of pre-damaged PFUs at various damage levels (crack network and melted droplets) was carried out under high heat load conditions with several hours of cumulated plasma duration. IR data and preliminary surface analyses show no evidence of significant degradation damage progression under these conditions.

1. Introduction

One of the main goal of the WEST project [1] is to test the ITER technology for the divertor Plasma Facing Units (PFUs), which consists

of massive tungsten (W) monoblocks (MBs) bonded on a CuCrZr cooling tube, with ≈ 0.5 mm toroidal gaps between blocks (intra-PFU gap) [2]. The heat exhaust capability provided by the pressurized water cooling circuit are $10 \cdot MW.m^{-2}$ steady state, up to $20 \cdot MW.m^{-2}$ for slow

^{*} Corresponding authors at: CEA, IRFM, F-13108 Saint-Paul-lez-Durance, France. *E-mail address*: yann.corre@cea.fr (Y. Corre).

See http://west.cea.fr/WESTteam.

transients (for a limited number of cycles). The parallel heat flux expected in the SOL of both, the ITER and WEST tokamaks, are very high, typically 200·MW.m⁻² in steady-state during full power operation [3] and more during disruptions. Using oblique intersection angles of the magnetic field lines (MFLs) with the top surface of the PFU, one can reduce the MB surface heat load by a factor of 20 (assuming an incident angle of $\alpha = 3^{\circ}$) in order to match the heat exhaust capabilities of these components. However, gaps between MBs and PFUs introduce leading edges (LEs) exposed to full parallel plasma flux and therefore prone to local overheating [4]. The gaps between PFUs (inter-PFU) and MBs (intra-PFU) lead to poloidal (yellow) and toroidal (blue) LEs respectively (see Fig. 1). The toroidal component of the magnetic field is perpendicular to the poloidal LE surfaces and parallel to the toroidal LE surfaces. At the output of the toroidal gap, the poloidal LE wetted area is extended deeper in the vertical direction because of the MFLs entering the gap. The image of the gaps on the leading edge, calculated by field line tracing code, are called "optical hot spots" (OHS). To observe the OHS impact in front of the toroidal gap of the downstream MB, few PFUs were installed shifted in the radial direction by + 1.5 mm and -1.5 mm, in the high field and low field sides respectively, to generate 3 mm maximum shift between them (as displayed in Fig. 1). The geometry is defined in the local frame of the PFU {x, y, z}, where x, y, z correspond to the poloidal, toroidal and vertical directions. Assessing the thermal loads and potential material damages (tungsten recrystallization, cracking and melting) on ITER-grade components is a key point for safe operation and divertor lifetime. ITER-grade refers to the W materials which comply with the ITER divertor requirements in terms of chemical composition, density, hardness as well as grain size and elongation perpendicular to the plasma facing surface (see ITER standard details in [5]). In this paper, we'll report on the operation of the ITER-grade PFUs in WEST up to the C7 experimental campaign (Jan-April 2023). It covers the whole of WEST phase I (C1-C5 experimental campaigns) and the beginning of WEST phase II experiments (C6-C7 experimental campaigns).

With phase II of the WEST project, the lower divertor is now fully equipped with ITER-grade actively cooled plasma facing units. The PFUs were mainly manufactured by AT&M (Advanced Technology of Materials, China) company using hot isostatic pressing (HIP) for bonding W blocks (armour thickness 6 mm) to CuCrZr tube with an intermediate Cu ring [7]. The divertor ring consists of 456 PFUs, each of them having 35 W blocks for which the width varies between 26 and 31 mm in the toroidal direction [7], from the inner to the outer sides, respectively. In total, the divertor target includes 16.000 W blocks that can be tested in WEST, which represents 5 % of the number of MBs foreseen in the ITER divertor. The WEST phase II configuration enables to run experiments with long plasma duration, relevant for testing the actively cooled components under steady state condition. During the last experimental campaign, (C7 Jan - April 2023), plasma discharges with a duration of

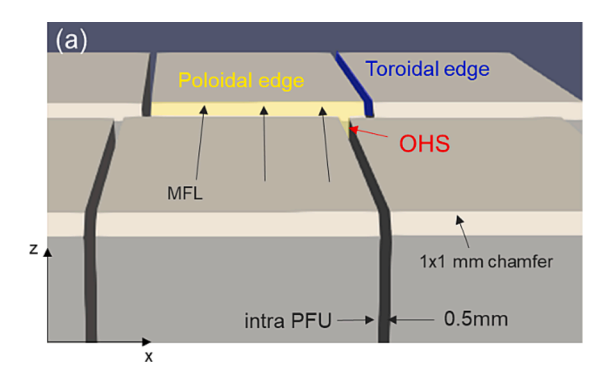
100 s were achieved, see Fig. 2.

In total (see Table 1), WEST could reach about 5.5 h of plasma and 43 GJ injected RF energy to the plasma, cumulated in 3 a months period (C7 Jan - April 2023). This is comparable to the energy values accumulated in Tore Supra in 2007-2008 where significant progress was achieved in the domain of steady-state tokamak research (10 h plasma time in both 2006 and 2007, with 65 GJ injected RF energy in 2006 and 40 GJ in 2007) [8]. Employing the long discharge capability, the ratio between accumulated plasma duration and number of disruptions decreased from 353 to 123 disruptions per hour of plasma during WEST phase I (C1-C5 experimental campaigns) and II (C6-C7 experimental campaigns), respectively. The plasma exposure achieved in WEST is, up to now, mainly characterized by steady state plasma conditions in the L-mode regime with attached divertor plasma conditions, where the electron temperature (T_e) lies between 20 and 40 eV on both inner and outer legs of the divertor. The progress made in term of steady-state tokamak operation (plasma duration and injected RF energy) is displayed in Fig. 2-a. The maximum RF power injected and coupled to the plasma, in a stable and reliable way, is currently 5 MW, mainly with Lower Hybrid launchers (LHCD heating system). Higher power has been coupled to the plasma during shorter duration because of plasma instabilities, leading to MHD activity and radiative collapse. The plasma heat flux achieved in a stable and reliable way on the top surface of the MBs on the outer strike point (OSP) is 6 MW.m⁻² (see Fig. 2-b), which represents 60 % of the nominal heat flux expected in ITER. The heat flux achieved on the inner strike line is typically a third of the value obtained on the OSP (thus 20 %of the nominal heat flux expected in ITER).

In this paper, the most recent progress regarding the evaluation of the heat loads on the ITER grade divertor components is presented, in particular in the toroidal gaps, on the poloidal chamfers and near trailing edges. Section 3 presents the MB surface shaping and assembling of the PFUs with each other. Section 4 presents the latest experimental and numerical results concerning the understanding of the damage mechanisms (W-cracking and melting) which appeared in WEST during phase I operation, when the divertor was equipped with a mix of Wcoated graphite and ITER-grade PFUs. Section 5 summarizes the plasma exposure of pre-damaged PFUs including various level of damages. Two PFUs have been taken out from the production batch and exposed in a HHF test facility (e-beam gun) to generate well controlled and different type of damages (micro crack, crack network, melted droplet) [9]. The pre-damaged PFUs have then been installed and exposed in the WEST tokamak to investigate the impact of damaged MBs on plasma operation. Predamaged PFU#1 was exposed to C3 and C4 and Predamaged PFU#2 was exposed to C7 WEST experimental campaigns, respectively.

2. MB Shaping and PFU assembling

To protect the LE of the MBs from premature damaging, ITER has



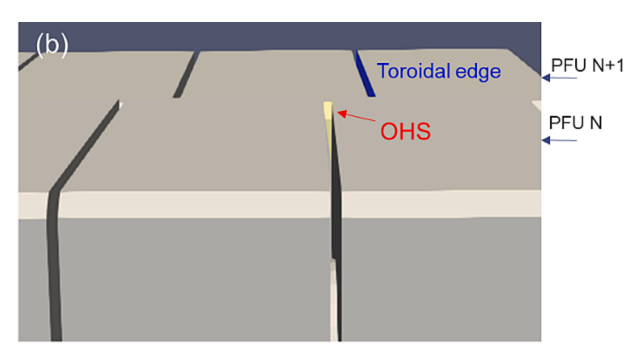


Fig. 1. Two consecutive PFUs with (a) the flat top geometry (WEST phase I) and (b) the 0.5 toroidal bevel geometry as foreseen in ITER to protect the poloidal LE. A chamfer (1 mm width, 1 mm height) can also be used on the LE to spread the power on broader surface in case of LE exposure [6]. Downstream PFU (N + 1) is shifted by 3 mm in the radial direction to get the impact of the OHS on the LE.

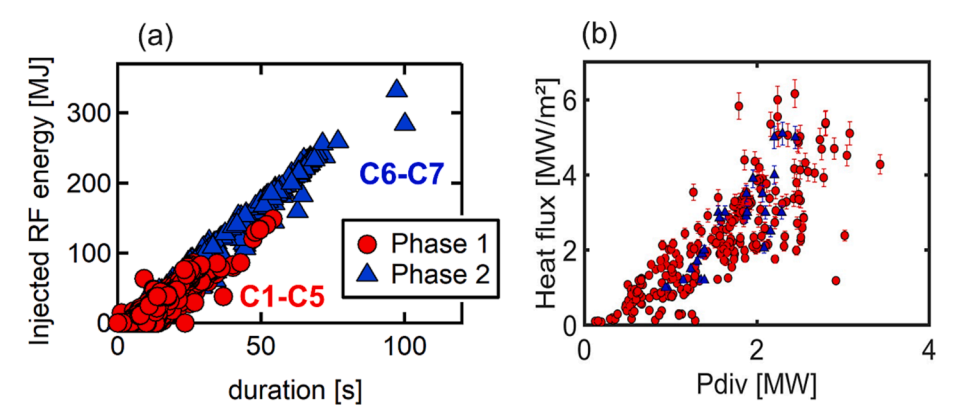


Fig. 2. (a) Injected RF energy as function of pulse duration during WEST phase I (red points) and phase 2 (blue points). (b) Peak heat flux on the OSP derived from embedded thermal sensors (TC and FBGs) as function of the power in the divertor ($P_{div} = P_{tot} - P_{rad}$). (For interpretation of the references to colour in this figure legend, the reader is referred to the web version of this article.)

Table 1Overview of the WEST achievements so far: number of plasma discharges, cumulated plasma duration, disruption and injected energy during WEST phase I and II

	Nb Plasma	Cumul (h)	Disruptions	W total (GJ)
Phase I	3890	7.3	2580	21.3
Phase II	1113	5.5	681	43

decided to shape the MB with a 0.5 mm height toroidal bevel [2], see Fig. 1 (b). In ITER, the assembling tolerances are set to \pm 0.3 mm vertical misalignment between two consecutive PFUs (δ) to prevent overexposed LEs over the full divertor surface [10]. Two MB geometries have been already tested in WEST with different misalignments, typically above and below ITER specification (\pm 0.3 mm assembling tolerance):

• The first geometry consists of the flat top MB shape used during WEST phase I, as shown in Fig. 3-a, with sharp or chamfered LEs. Here, the gyrating ions and electrons propagating along MFLs can strike the poloidal LE of MB at near normal incidence. The power deposited and consequently the temperature of the W on the LE depend strongly of the alignment between the concerned MB with the adjacent upstream MB. With strong misalignment ($\delta=0.8$ mm, maximum value measured during the C3 experimental campaign), the surface temperature, evaluated with the IR thermography system, reached values of up to 900 °C [11] on sharp LE, with moderate and steady state parallel heat flux $q_{//}\approx50$ ·MW.m $^{-2}$ (assuming a uniform distribution in the poloidal direction). Post-mortem analysis of the PFU following the C3 experimental campaign, revealed that most of the LEs located both near and further away (where intense

steady state heat load are not expected) from the strike point areas exhibit clear W cracks and in some cases fine scale melting [12] despite only modest injected power levels during C3, however with a high number of power transients from disruptions.

- With misalignments up to the assembling tolerance foreseen in ITER $(\delta < \pm 0.3 \text{ mm})$, as operated in the WEST C4 experimental campaign, the surface temperature reached values of up to 1200 °C on both sharp and chamfer LEs [13] in dedicated high power plasma experiments using LHCD heating only ($P^{inj} \approx 4$ MW), therefore with higher parallel heat flux $q_{//} \approx 100 \text{ MW} \cdot \text{m}^{-2}$ than measured during the C3 experimental campaign [14]. In the C4 experimental campaign, higher temperature, (close to 2000 °C on the sharp LE), has occasionally been measured during high performance plasma operation $(P^{inj} \approx 8 \text{ MW})$ using both ICRH and LHCD systems, only after fresh boronisation when the radiated fraction is reduced down to 30 % for several discharges [15]. Post-mortem analysis following the C4 experimental campaign showed that the damage on the tungsten blocks created during C3 did not further evolve during C4, suggesting that the damage indeed resulted from singular events rather than continuous heating due to steady state operation [16].
- As second geometry a 0.5 mm height toroidal bevel was introduced for MB installed in phase II with sharp or chamfered LEs (see [6]), as shown in Fig. 3-b. In this case, the ions and electrons cannot strike the poloidal LEs except in front of the toroidal gaps where they can strike the LE of the adjacent downstream MB on a small area (<1 mm²), also called "optical hot spot" (OHS), see the OHS in 3D geometry in Fig. 1-b. Modelling of the heat flux and temperature of the MB at the ITER target plate PFU predicts that; hot ions released from the pedestal during ELMs could induce flash melting at the OHSs, depending on the plasma scenario and the alignment of the MBs with

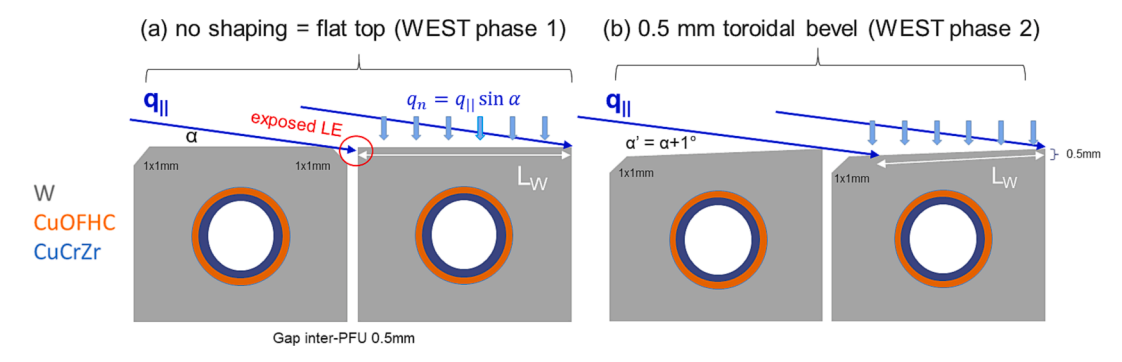


Fig. 3. MB geometry. (a) flat top and (b) 0.5 toroidal bevel with chamfer on the LE only as operated in WEST phase I and II, respectively. Magnetic field lines are shown in blue, the plasma wetted area in white. (For interpretation of the references to colour in this figure legend, the reader is referred to the web version of this article.)

respect to each other [4]. The main drawback of the MB shaping is the reduction of the wetted area (where L_w is the wetted length) and the increase of the MFLs surface inclination angle (+1°). Assuming $\alpha=3^\circ$ and geometrical projection of the parallel heat flux onto MB surfaces, this corresponds to ≈ 20 % higher heat flux on the top surface. Furthermore, vertical misalignment may change the wetted area and consequently, the surface temperature and mechanical stresses in the MB.

3. Heat load on castellated MB

3.1. Experimental set-up and method

Accurate measurement of the tungsten temperature is required to evaluate the heat load on the PFUs.

WEST is equipped with an extensive set of diagnostics for heat load measurements especially in the lower divertor. Infrared thermography systems have been deployed on the top part of the machine to monitor the temperature of the component on the lower divertor. They currently consist of five endoscopes providing a broad view of the divertor sectors with a spatial resolution ranging between 3 and 5 mm per pixel [17] and one endoscope with a reduced field of view (few MBs) at a very high spatial resolution of 0.1 mm/pixel [18]. Because of the low emissivity of tungsten, which depends on various parameters such as wavelength, temperature, surface structure and chemical composition, it is very challenging to derive the PFU temperature during plasma experiments [19]. To complement the IR thermography, some PFUs are equipped with embedded temperature sensors such as thermocouples (TCs) and multiplexed fiber Bragg gratings (FBGs), which provide up to 11 and 15 spot measurement points per fiber a few mm below the surface, during phase I (W-coated graphite PFUs [20]) and phase II (ITER-grade PFUs [21]), respectively. Thermal inversion of the sensor measurements enables to derive the heat flux distribution (peak heat flux and heat flux decay length λ_0) as function of time [22].

Based on the embedded sensor measurements, a method has also been developed to measure the emissivity of the W-coated graphite divertor tiles directly in the WEST tokamak [19]. The method relies on the double heating method and takes advantages of the divertor temperature increase after successive plasma experiments due to the inertial behavior of the plasma facing components. Strong variation of the emissivity (up to a factor of 4) along the divertor tile was measured during the C4 experimental campaigns [23]. Using the emissivity measurements performed between pulses, it is then possible to evaluate the temperature on the top surface of the PFU based on the IR data and to compute the heat flux using thermal inversion [24]. Infrared thermography and embedded sensors return equivalent values of energy absorbed by the divertor PFUs over a large variety of plasma scenarios. However, some discrepancies are found on the evaluation of the peak heat flux and heat flux decay length (λ_0). Peak heat flux and λ_0 values obtained with embedded sensors are usually lower and larger than those estimated from IR data, respectively. The heat flux decay length at the target is found to scale mainly with the magnetic flux expansion through the variation of the X-point height [14]. The peak heat load reported on shaped W-coated graphite PFUs during WEST phase I (C1-C5 experimental campaigns) reached up to 6 MW m⁻² during standard high RF power operation with typically 5 MW of additional heating, see Fig. 2-b. Assuming that ion and electron propagate along the MFLs with no gyration and no drifts, also called guiding center or optical approximation (OA), the heat flux deposited on the target (q_n) can be expressed as the geometrical projection of the parallel heat flux $(q_{//})$ onto the target:

$$q_n = q \| \sin \alpha \tag{1}$$

where α is the incident angle of the magnetic field with the MB surfaces. Assuming an incident angle $\alpha=3^\circ,$ the parallel heat flux derived from equation (1) would be 120 MW·m $^{-2}$ at maximum in the WEST tokamak based on PFC temperature measurements on the outer

strike point (OSP). Because a significant fraction of the heat flux is being reflected by the W surfaces (about 50 % backscattering of the electrons is usually measured in high heat flux test facilities), an even higher parallel heat flux can be expected in the SOL, i.e. up to $150-200~\mathrm{MW}\cdot\mathrm{m}^{-2}$.

3.2. Impact of the MB shaping on the temperature distribution

On the ITER-grade PFUs featuring the flat top geometry, the heat load is lower by typically 20 % compared to the bevel geometry (α '= α + 1° as seen in Fig. 3). Fig. 4 displays IR images of the MBs top surface without (flat top geometry) and with MB shaping (0.5 mm toroidal bevel as foreseen in ITER) obtained under similar plasma conditions (4 MW injected RF power, $I_p = 500$ kA, B = 3.7 T). The two pictures show very different IR emission patterns. During phase I (left), very high temperatures were observed on the poloidal LE as also reported in [13]. Taking into account the emissivity values obtained from post-mortem measurements [23], the apparent or black-body (BB) temperature ($T_{BB} \approx 600$ °C assuming $\epsilon = 1$) can be corrected to derive estimate of the true temperature on the LE, $T_{LE} \sim 900$ °C (assuming $\epsilon \approx 0.4$ which is the averaged value measured on middle part of the top surface and used in [11]) or $T_{LE} \approx 1200$ °C (assuming $\epsilon \approx 0.2$ as measured near the LE).

During phase II (right), very complex and different IR emission pattern was observed in particular near the edges of the MB. On the top surface, magnetically shadowed (left part of the MB) and wetted areas (right part of the MB) are clearly separated, well in line with numerical modelling of the heat flux taking into account also the toroidal bevel. Nevertheless, a higher IR signal is measured near the 1 mm chamfer (on the poloidal LE located in the magnetically shadowed area, thus not directly exposed to the SOL plasma), in the toroidal gaps (TGs) and trailing edges (TEs) of the MB. The maximum apparent temperature is seen in the TGs with no tungsten material, attributed to the Planck radiation emitted from the cavity ($\varepsilon\approx 1$), which is heated up by the lateral sides of the MB. For similar plasma conditions, apparent temperatures are smaller for the shaped ($T_{BB}\sim 250~$ C at maximum) compared to the unshaped MB ($T_{BB}\sim 600~$ C at maximum) demonstrating the clear benefit of the MB shaping for the temperature response of the MB.

3.3. Optical hot spot (OHS)

A major concern for ITER is also the penetration of the ions and electrons in the toroidal gaps by their gyro-motion, as shown in Fig. 1-b and depicted in [4]. The resulting heat load on side faces near the gap entrance can be very intense of the magnitude of the parallel heat flux because of the almost 45° or perpendicular angle for chamfer and sharp LE, respectively, on this surface (red circles in Fig. 5). A series of 6 consecutive PFUs were installed with deliberately misaligned MBs in the poloidal direction (1.5 and 3 mm shifts) to generate amplified thermal signatures of the OHS on the 45° inclination chamfer of the adjacent downstream MB. A dedicated experiment has been performed with discharges in which the outer strike line was placed on top of the toroidal gap in order to maximize the heat load and temperature increase on the OHS. Fig. 5-a shows the VHR IR image obtained when the temperature of the MB reaches thermal equilibrium and for comparison Fig. 5-b a photo of the component to show the chamfer on the poloidal LE and the poloidal misalignment between PFU#8 and #9 (≈ 1.5 mm shift). As shown in the previous sub-section, the toroidal gaps exhibit higher IR signals. On the downstream MB, one can see a small hot spot, not aligned with the toroidal gap (0.8 mm away from the theoretical OHS position as measured by the VHR IR camera). The question is whether this represents a real hot spot that is shifted because of physicsrelated effects or simply a reflection on the W-facets?

3.4. Photonic modelling of the thermal scene

To understand the IR measurements and the origin of hot patterns along the toroidal gaps, an end-to-end simulation has been used to

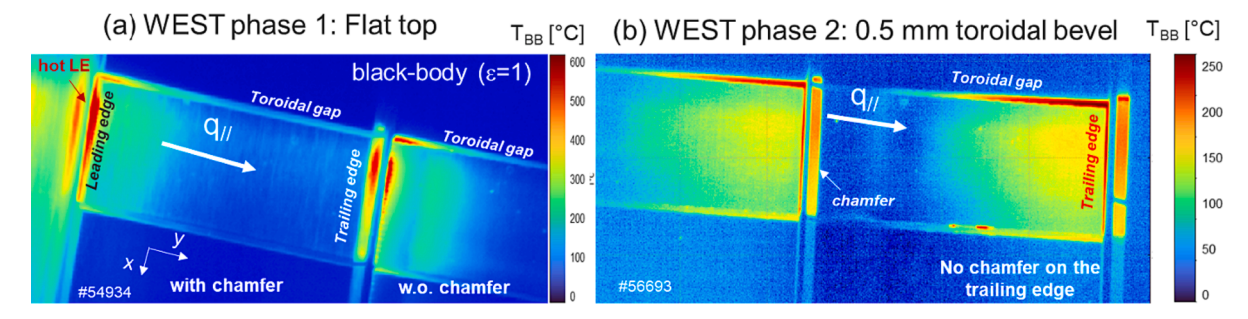


Fig. 4. Apparent temperature maps obtained with the VHR system during phase I and II with flat top (a) and toroidal bevel (b) geometries ($\epsilon = 1$, black-body temperature).

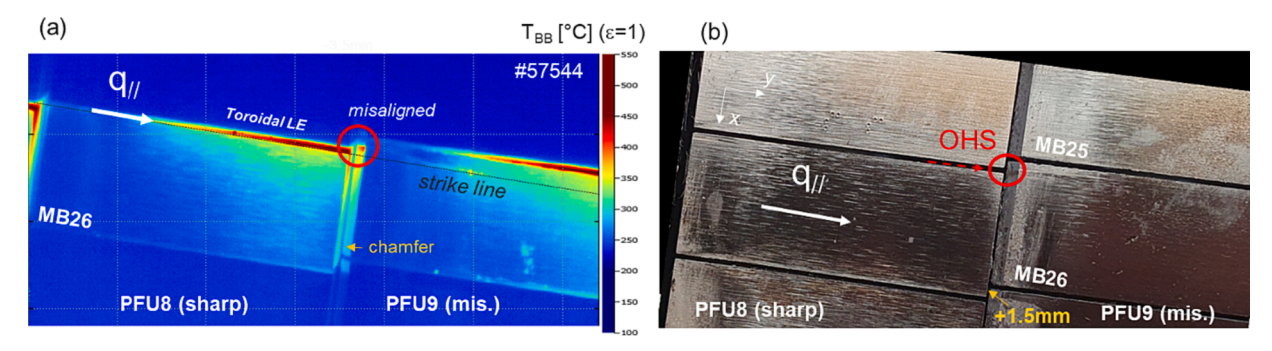


Fig. 5. (a) Apparent temperature map obtained with the VHR system with + 1.5 mm poloidal misalignment between PFU#8 (sharp LE) and #9 (ϵ = 1, black-body temperature). (b) Picture of the same blocks taken after plasma exposure (shutdown following the C7 experimental campaign, 2023).

simulate the recorded IR images from a given thermal scene. Such a simulation is based on a Monte Carlo Ray tracing code able to model the light behavior in 3D complex geometry taking into account the photonwall interaction and to reproduce the camera view from a camera model [25]. In a first step, only geometrical parameters of the camera are modeled, i.e. the field-of-view and pixel resolution. Blurring effect is applied in a second step to take into account optical effects as diffraction and aberrations. The ray tracing inputs are the thermal scene (temperature of the component predicted by theory) and the optical properties of the W-surfaces. In the simulation presented here, the thermal scene is fixed and is the results of heat load computations, only the optical properties are variable to fit simulated images to experimental images. The thermal scene is computed in two steps: the first step consists of modelling the heat load (q_n) on the MB surface with the magnetic field line tracing code (PFCflux code [26]). The second step consists of computing the resulting surface temperature from a 3D Finite Element Modelling code (ANSYS). The optical properties materials are characterized by the emissivity values and by the bidirectional reflectance distribution function (BRDF) which describes how incident light is reflected on the metallic surface. In the following simulations, the emissivity values were taken from emissivity measurements (in-situ and laboratory measurements [23]) and the reflectance model used is a linear combination of diffuse (25 %) and Gaussian specular (75 %) reflection components controlled by two coefficients in the simulation. Fig. 6 displays the comparison between experimental and simulated VHR IR data. The simulation replicates well the overall pattern and some conclusion can be drawn:

 In the toroidal gaps, simulation shows that multi-reflection ("cavity" effect) could generate intense IR signal consistent with the experimental data.

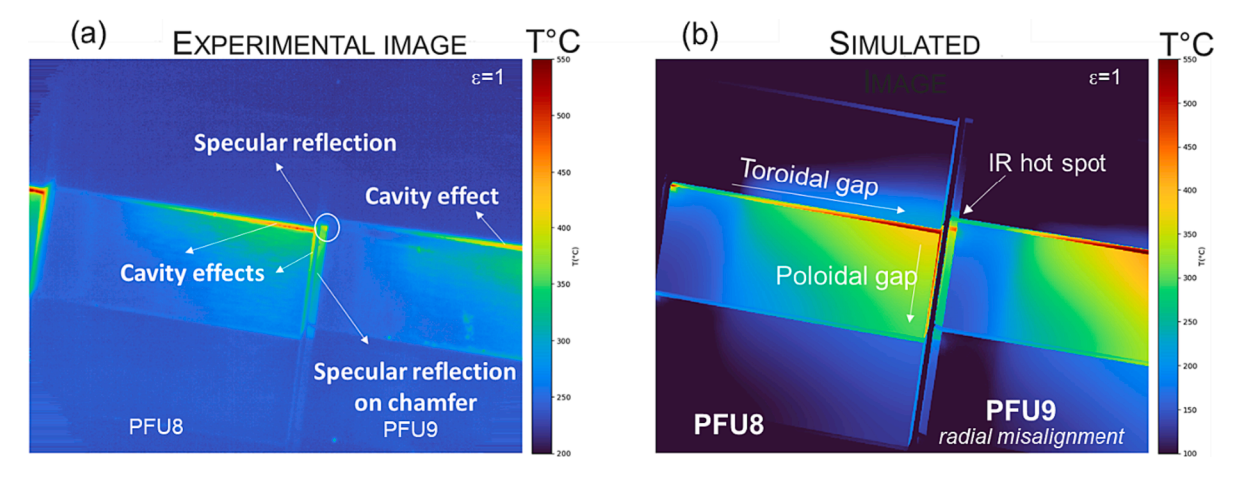


Fig. 6. Experimental (a) and synthetic (b) IR image taking into account plasma heat load footprint and multi-reflection on the different W-surfaces (MB sides, chamfer, trailing edge...).

- Specular reflection of the thermal radiation emitted by the back side
 of the MB (trailing edge) on the 45° inclination chamfer of the upstream MB can generate "false" hot spot (not representative of the Wtemperature).
- Near the OHS theoretical position, a hot pattern, which can be confused with OHS thermal signature, is observed: this comes from the specular reflection of the light trapped in the toroidal gap that is superposed to the reflection of the back side of the MB as mentioned before. This also leads to the "false" IR hot spot which is not aligned, about 2 mm away from it, with the toroidal gap as shown in the Fig. 6-b
- The thermal signature of the OHS is not detected with the VHR IR system possibly because it happens in the cold part of the MB, in the magnetically shadowed area. Therefore the thermal signature of the OHS is probably too low compared to the reflection from hot part of the upstream MB (on the trailing edge, part of the MB top surface which is fully exposed to the plasma heat load). Theoretical model (based on OA) predicts an increase of temperature of a few ten degrees due to OHS. Experimental images confirm that there is no increase of temperature due to OHS, and we prove thanks to simulation that the observed hot patterns comes from special behavior of photon as cavity effect in gaps or specular reflections on trailing edges or chamfer.

This study shows the interpretations of IR images is difficult and should be analyzed with caution. It is worth noted that WEST VHR coupled to detailed simulation allows us to discriminate real temperature of the W-surfaces to cavity effect or reflections. In the case of poor resolution, it will be very difficult to separate the two effects.

4. Tungsten cracking and melting on poloidal LEs

The consequence of W-cracking and melting on plasma operation is a high priority issue for ITER. Several tokamaks using tungsten as divertor material such as TEXTOR, JET, AUG, EAST or DIIID have already produced a large set of data showing different kind of damages in different geometrical configuration (magnetic equilibriums, plasma exposures and PFC geometries). Inspection of the Div-III divertor tiles in AUG reveals deep cracks through the target, shallow cracks in the high heat load region and strong local damages on protruding tiles [27]. Dedicated experiments have also been successfully carried out, in both limiter and divertor geometries, to investigate sustained (TEXTOR) [28] or transient ELM-induced melting of tungsten PFC of special geometries, such as exposed leading edge (LE) in JET [29] and AUG [30], as well as sloped lamella in JET [31] and AUG [32]. Except the EAST tokamak, these experiments have been performed with bulk tungsten and no active cooling such as ITER-grade PFU, therefore with a strong dependence on surface temperature and pulse history (full modelling of the pulse is usually required to get proper temperature gradient in the component).

4.1. W-cracking post-mortem observation (C3 experimental campaign)

During phase I operation, inspection of the ITER-grade PFUs after the C3 experimental campaign revealed traces of damages (cracks, fine scale melting) at both leading and trailing edges of the MBs. During the assembly of the targets on the test sector, some ITER-grade PFUs were vertically misaligned (up to 0.8 mm at maximum). With the flat top MB geometry, the LEs were not protected and directly exposed to the parallel heat flux leaving its footprint on the W-surfaces, mostly on the MBs located near the outer and inner strike line positions where plasma heat load is the highest. A picture taken on the MB LE with an electronic microscope is shown in Fig. 7-a. For this MB, surface metrology reveals 0.8 mm vertical misalignment with the upstream MB. This value which exceeds the ITER tolerance for assembling (\pm 0.3 mm) is interesting, nevertheless, to maximize the plasma footprint of the W-surface when the steady-state plasma heat load is small (as it was the case during C1-

C3 experimental campaigns). The damaged area observed with the electronic microscope is consistent with the surface metrology, here we measure 0.8 mm vertical extension all over the LE. The cracks are distributed in the poloidal direction and exhibits vertical extension suggesting normal stress aligned with the tube direction (parallel to the grain orientation). The mean space between cracks is 0.4 mm on this MB as well as the other MBs with overexposed LEs in the machine [16]. OHSs were also evidenced in front of the toroidal gap on the downstream MB [12], confirming the numerical simulations [4], although their impact on the operation and the lifetime of the components was limited.

Damage may be induced by different processes which can lead to: brittle fracture below the Ductile to Brittle Transition temperature (DBTT) or ductile failure for which softening (recovery / recrystallization) process plays a major role. To improve our understanding in the damage mechanism, a numerical tool has been developed (TREX code [34]) to assess W crack formation considering experimental heat flux, mechanical properties (elastic-viscoplastic) and softening of the tungsten material. Simulations have been performed assuming quasi steadystate (from 45 MW/m² to 70 MW/m² parallel heat flux as measured in WEST during phase I [12]) and disruption loading (impact heat flux factor HFF of 30 MW·m $^{-2}.s^{-1/2}$, assuming $q_n=600~\text{MW·m}^{-2}$ peak heat flux) [35]. The disruption thermal cycle is composed of 3 ms heating including a ramp up for 1 ms and a ramp down for 2 ms which is representative of thermal quench duration in ASDEX upgrade [33], since we don't have yet accurate measurement of the thermal quench duration in WEST. Simulation performed with steady state heat load, with or without disruption loading on top of it, doesn't show any overstress regarding the material yield stress (Ys). Only accumulated plastic strain could lead to failure after significant number of thermal cycles (several thousands).

Potential overstress is observed only if we consider the disruption alone (without steady-state heat load preceding the disruption event), with PFU temperature before disruption equal to the water temperature (70 °C). The normal stress (σ_{ND}) is maximum along 88 % of the leading edge for this simulation at 5 ms after the disruption. Fig. 7-b shows the evolution of the maximum temperature and stress gradients in the normal direction (along the cooling tube axis, x axis in the local frame of the PFU), at the center of the LE (computed by TREX). Boundary conditions and thermomechanical properties assumed in this modelling are similar to the ones used in [35]. The normal stress (σ_{ND}) evaluated by TREX exceeds the material yield stress (Y_s) during the cooling phase (>2.5 ms) when temperature decreases below the DBTT. Brittle failure is expected based on the numerical assessment. A metallographic study (especially to observe the rupture surface) is planned to confirm the modelling and failure mechanism.

4.2. W-cracking in-situ detection (C5 experimental campaign)

W-cracking has also been evidenced during steady state plasma operation with the VHR IR system on one particular MB with a deliberately overexposed leading edge positioned in remote area (MB#28) for dedicated exposure. A 2 mm deep groove were used on the upstream MB (see Fig. 8) to reach W-melting point on the sharp LE of the downstream MB [36]. One experimental session was dedicated for this purpose. The strike line was positioned on MB#28 using a high X-point magnetic configuration (while usual strike line position is between MB#24 and #26) and the power was increased step by step until melting point is reached. The cracks initiate with an injected LH power of 4.6 MW when the LE temperature was about 2600 °C. Five cracks were detected during the cooling of the component, when the temperature becomes more uniform on the top surface. The multiple reflection of the light inside the crack leads to an enhancement of the local emissivity and apparent temperature as depicted in the previous section and shown in Fig. 8-a. The apparent temperature increase in the crack is only few tens of degrees because the crack widths are smaller than the pixel size, it is

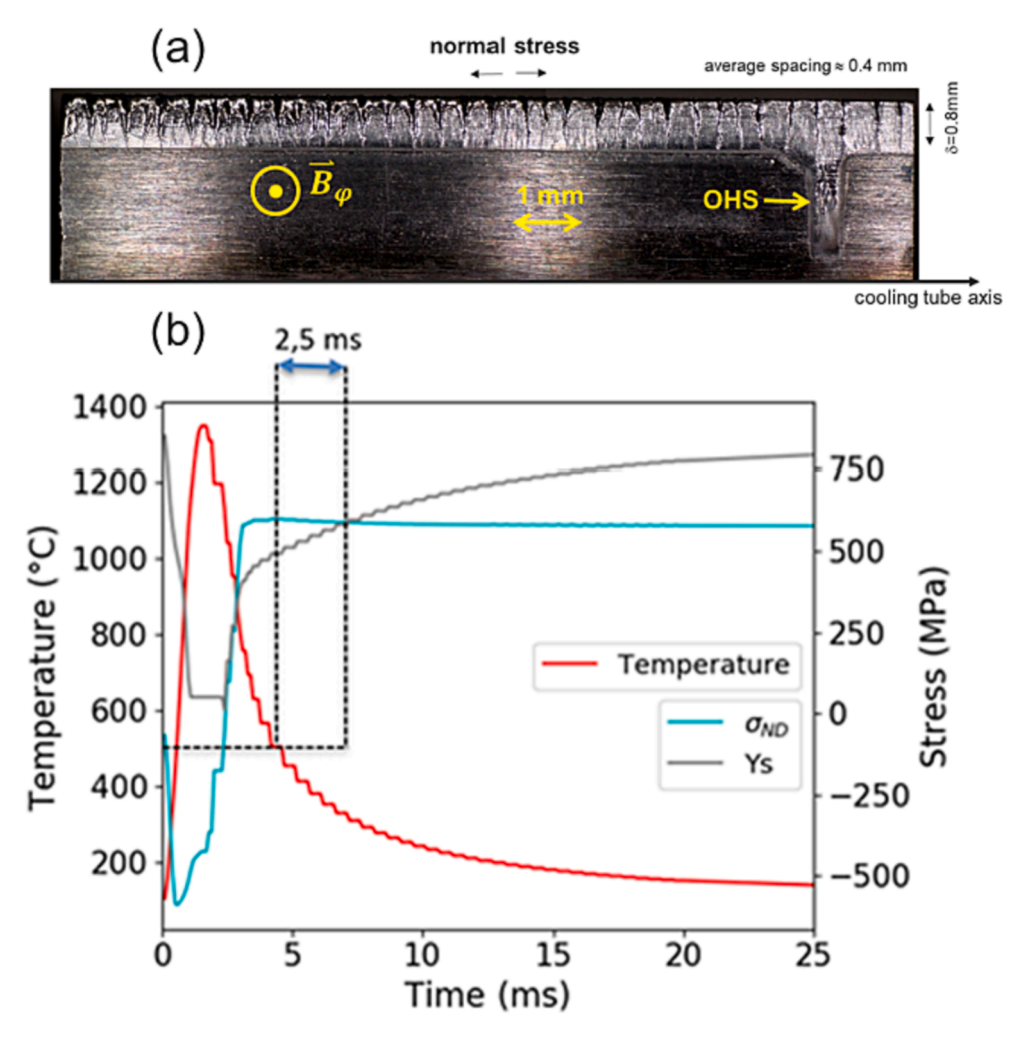


Fig. 7. (a) Post-mortem observation (electronic microscope) on the misaligned poloidal LE without and with OHS taken from [12]. Footprint of the misalignment showing W-cracks and OHS in front of the toroidal gap of the upstream MB. (b) TREX simulation showing temperature (red) variation, material yield (Ys, gray) and normal stresses (σ_{ND} , blue) as function of time for 1.8 MJ/m² disruption (0,8mm misaligned LE) taken from [33]. (For interpretation of the references to colour in this figure legend, the reader is referred to the web version of this article.)

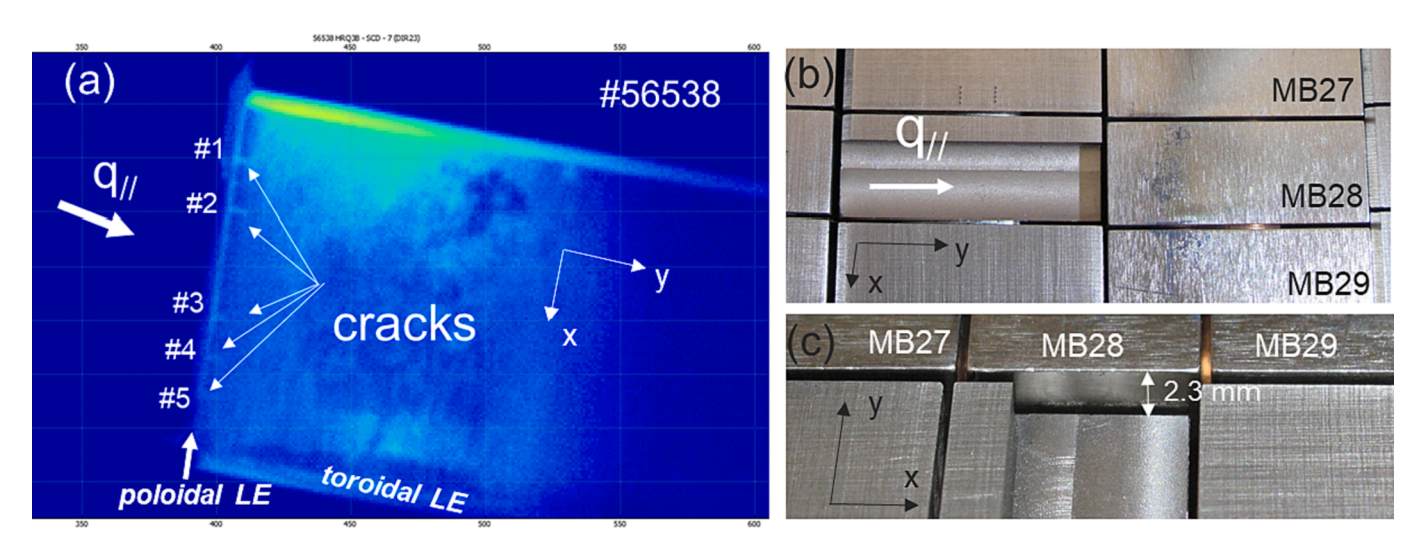


Fig. 8. (a) IR view of MB28 PFU#8 (sharp leading edge exposure) during cooling phase (T° on top surface is about 300 °C). Picture of the overexposed MB with the groove on the upstream block, top view (b), front view (c).

therefore not detectable during the heating phase when the temperature is high and non-uniform.

After removal of the PFU from the tokamak (shutdown between C5 and C6 experimental campaigns, 2021), confocal microscopy measurement performed on the MB shows that the crack width lies in the range of 26 μm and 77 μm , thus smaller than the IR pixel size (100 μm) as speculated earlier. They propagate over 0.3 to 2.5 mm in the toroidal direction on the top surface which is consistent with IR measurement [37]. The stress and strain are evaluated by the TREX code based on experimental boundary conditions during steady state plasma operation [34]. The heat load distribution on the block surfaces is determined with the IR measurement and 3D FEM modelling of the heat transfer in the component (ANSYS code). Parallel heat flux of about 90 MW.m $^{-2}$ was required to reach 2600 °C on the LE as measured with the VHR IR camera (#56535) [37].

Based on the thermal inputs derived from IR temperature measurements (#56535, $I_p=500kA,$ X-point height dX =110 mm, $P_{LH}=4.6$ MW), the thermomechanical simulation predicts between 1 and 5 heating/cooling cycles before crack initiation at the maximal plastic strain position (ductile failure). About 9 pulses with similar heat load were performed before W-cracking were detected with the IR system [37]. Contrary to the previous case where brittle failure is expected, ductile failure can occur under extreme heat loading focused on a sharp LE. Such extreme loading condition are not expected to happen in ITER if the plasma heat load limitation, PFU heat exhaust capabilities and assembling tolerances are fulfilled.

4.3. Sustained W-melting (C5 experimental campaign)

No impact on the main plasma was observed in JET despite a strong increase of the local W source consistent with evaporation, while more detrimental effects were observed in AUG (W ejection followed by disruption [32]). To complete previous melting studies, sustained melting of W on actively cooled ITER-grade PFU have been executed in WEST (C5 experimental campaign, Dec. 2019) using the groove geometry on the upstream MB as presented in Fig. 9. Controlled and sustained W-melting has been achieved during three consecutives pulses for about 5 s duration each [36].

The experiment has been modeled in full detail with the MEMENTO code to simulate the melt dynamics taking into account the cooling pipe system [38]. The observed melt displacement pattern is due to the melt flow in the $J \times B$ direction (inboard if the melting occurs on the outer strike line with forward magnetic field), where J is the replacement current generated by the thermionic emission. The melt layer remains

very thin (about 10 µm) and moves slowly due to high viscous damping $(\propto\!1/h^2,$ h being the pool depth). The melt dynamics in WEST [39] are therefore distinguished from transient melting observed in JET and AUG tokamaks [40]. The main differences are summarized in the Table 2, where $\langle J \rangle$ stands for the depth-averaged replacement current density component responsible for the main driving $J \times B$ force [31].

The melting has been detected with the VHR IR system when the sharp LE becomes deformed as illustrated in Fig. 9 (typically between 1.2 and 2 s after RF power is applied). MEMENTO simulations show that melting point is reached shortly after 1 s, and the deformation profile evolves promptly over the first second of the pool's life-time [39]. The crater depth is $\sim 10~\mu m$ at 1.2 s, increasing to $100~\mu m$ at 2 s, value which is equivalent to one IR pixel and therefore in agreement with the deformation detected by the IR camera, see Fig. 9. At the end of the exposure, crater depth and hill height reach about 200—300 μm , resulting in 0.26 mm $^{-3}$ of displaced material, fully consistent with the post-mortem measurements. Thus, within the uncertainties of the experiment heat flux input, MEMENTO modeling reproduced the final deformation profile as well as the novel experimental constrain - empirical timing of the melt onset.

The MB has received 2.8 kW of power during 5 s. Among the different surface cooling processes, the heat flux due to thermionic emission is the dominant one. However, unlike other W-melting experiments [41], thermionic cooling is merely ~ 2 times stronger than the radiative one as surface temperature exceeded melting point by only $\sim 10\,^{\circ}\text{C}$. While about 14 kJ energy was deposited over the full 5 s melting sequence, only a few Joules are required to melt the 0.26 mm $^{-3}$ W volume, resulting in high sensitivity of the melt production to minimal power variations [39]. Indeed, if the heat flux employed in the modelling of this experiment (with the decay length $\lambda_q=2$ mm and $q_{//}\sim 150$ MW.m $^{-2}$), is increased by 10 %, MEMENTO predicts a four-fold increase of the melt volume. This is the goal of the next melting experiment planned in WEST (C8 experimental campaign).

5. Plasma exposure of the HHF predamaged PFUs

5.1. ELM type damages

To test the ageing of the ITER-grade PFUs on an accelerated basis, it was proposed during the start-up of the WEST project, to damage in a controlled way selected MBs in the Judith 2 high heat flux (HHF) facility to evaluate the impact on plasma operation. The pre-damaged PFU program carried out in WEST is phased in time, with progressive increase of the damage type as well as plasma heat load and exposure time

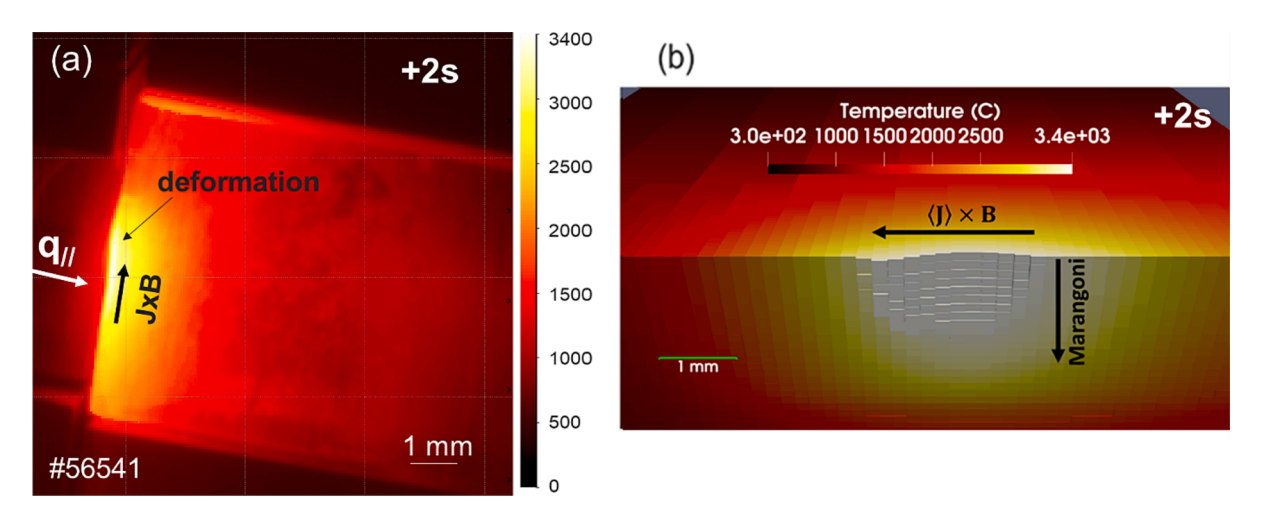


Fig. 9. (a) IR images during W-melting experiment at 2 s after RF heating is applied in the machine. Rounding of the poloidal LE is used to determine the time when the melting is reached. (b) MEMENTO simulation [31] output at the same timing showing the melt displacement, crater on the strike line and hill few mm away in the JxB direction. Direction of J × B and dominant Marangoni component are also illustrated.

Table 2Comparison of loading and melt characteristics in AUG and JET experiments [40] vs WEST experiment [39].

Melting	Loading	Pool depth	Pool lifetime	$\langle \mathbf{J} angle$	В	Melt displacement	Melt velocity
Transient	$q_{//}^{max}$ 1GW/m ² ELM, 3 ms	100–300 μm	10 ms	$2.5 - 3.8 \text{ MA/m}^2$	2.5—2.9 T	1–2 cm	1-2 m/s
Sustained	$q_{//}^{max}$ 150 MW/m ² Steady	10 μm	5 s	$1.3~\mathrm{MA/m^2}$	3.96 T	2–3 mm	~1 cm/s

to minimize the risk during the operation of the WEST tokamak. The procedure executed to get the first pre-damaged PFU is described step by step in [9], from test samples, prototype full scale and integration in the tokamak. Transient loads, representative of Type I ELM heat loadings, of an absorbed power density of L = $0.14 - 0.55 \, \text{GW/m}^2$ and a duration of 0.48 ms (impact heat flux factor HFF = $3 - 12 \, \text{MW/m}^2$.s^{1/2}) are used at a repetition rate of 25 Hz to achieve a total of 10^5 thermal cycles [42]. The resulting pre-damage exhibits micrometer-size crack network and high roughness on the tungsten monoblock (MB) top surface. Fig. 10 shows the three kinds of damages generated by the ELM-thermal cycle and tested in WEST: small cracks are generated by small ELMs (type #1), crack networks are generated by larger ELMs (type #3). Predamaged PFU#1 and PFU#2 were exposed in WEST phase I (C1-C4 experimental campaigns) and phase II (C6-C7 experimental campaigns) respectively.

5.2. Plasma exposure of the predamaged PFUs

Two predamaged PFUs have already been exposed in the WEST tokamak: the first (PredPFU#1) was exposed in WEST during phase I with the flat top PFU geometry (experimental campaigns C3-C4) and the second one (PredPFU#2) was exposed in phase II with the toroidal bevel geometry (experimental campaigns C6-C7). Fig. 11 shows the damaged MBs before plasma exposure for the two predamaged PFUs exposed in WEST. Only half part of the MB surface was loaded with the e-beam gun to keep a reference point next to the damaged area.

Predamaged PFU#1

A total of 10 MBs, equally distributed on the low and high field sides of the lower divertor, have been pre-damaged among the 35 radially aligned MBs of the WEST PFU. A first plasma exposure was carried out with small heat load in both inner and outer parts of the PFU ($q_{n} < 1\,$ MW.m⁻²) to avoid compromising the C3 experimental campaign [9]. Then it was decided to move the pre-damaged component to the highest heat load area for the following experimental campaign (C4 June-October 2019). The results of the C4 plasma exposure are detailed in [43]. In total, the PFU has been exposed in WEST to 7.3 h of cumulated plasma, including 2580 transient events (disruption) as presented in Table 1. Considering the strike line position as function of the radial position (MB number), MB24 with no damage was the most exposed one. MB26 featuring crack network was the second most loaded one, the outer strike line was connected to MB26 for \sim 45 min in total. A dedicated exposure with the outer strike line on MB#26 has been done with high RF power operation to maximize the surface temperature and mechanical stresses in the damaged MB. The pulse duration is typically 27 s, in which LHCD systems delivers 4 MW steady-state power during 20 s (about 90 MJ RF and ohmic energy coupled to the plasma per pulse). Plasma parameters are: plasma current Ip = 500 kA, toroidal magnetic field B = 3.7 T, line-averaged density, $\langle n_e \rangle = 4 \times 10^{19} \text{ m}^{-2}$. The temperature derived from the VHR IR system gives 400 °C in the predamaged area (middle part of the MB) and 900 °C on the chamfer of the poloidal LE (see Fig. 12-a) assuming an emissivity of 0.3 as measured in post-mortem in erosion areas [44]. 3D FEM modelling was then used to evaluate the heat loading during plasma exposure. To match the experimental temperature profiles in the toroidal and poloidal direction, we found heat flux $q_n = 5 \text{ MW.m}^{-2}$ with 12 mm heat flux decay length on top surface of the target ($\lambda_q=12$ mm). About 30 plasma discharges have been repeated during the experimental session (600 s and 1.9 GJ

cumulated exposure time and energy delivered to the plasma) and no consequence on the PFU and plasma operation were observed. The predamaged PFU was then removed from the WEST tokamak to carry out post-mortem measurement. On the "pre-damaged" area, we observed clear broadening of the cracks and further roughening. On the "healthy" area of the top surface of the MB, next to the e-beam loaded area, we observe new and potentially deep cracks in the poloidal direction [43]. Compared to the "healthy" area, precracking could reduce surfaces stresses that may accumulate due to a castellation of the area in smaller sections (crack network pattern). Thermomechanical modelling is required to make proper interpretation.

Predemaged PFU#2

The second predamaged PFU includes only one damaged MB with more severe type of damage (type #3), featuring crack network and melted droplets as shown in Fig. 11. The damaged block was positioned in the high heat load area on a monoblock (#25) accessible with the standard magnetic configuration (dX = 60 mm) to maximize both thermal cycles and plasma exposure time. The component was exposed during the C7 experimental campaign (Jan-April 2023) featuring long discharge capabilities with the fully actively cooled divertor. About 5.5 h of plasma duration was cumulated over 1113 pulse discharges (see table I and Fig. 2). At the end of the C7 experimental campaign, 4 weeks of operation were dedicated to repeat as much as possible high particle flux and long discharges in order to investigate the impact of the particle fluence on the ITER-grade components. A total deuterium fluence of 2.10^{26} D/m² and 5.10^{26} D/m² have been cumulated during the first part of the campaign and during the high fluence campaign, which is equivalent to the fluence expected during one or few ITER PFPO pulses.

The outer strike line was connected to the damaged MB during most of the campaign. Fig. 12 displays the VHR IR data for the predamaged PFU#1 (unshaped) and PFU#2 (unshaped). The IR images show two different patterns: the maximum of temperature is located on poloidal LE and on the wetted part of the top surface for the flat top (left) and bevel (right) geometries respectively. Because of the 0.5 mm height toroidal bevel, the heat load deposited on top surface of the MB was 20 % higher on the "shaped" compared to "unshaped" ITER-grade PFU used in phase I (flat top geometry), as explained in the introduction. Assuming a surface emissivity of 0.3 (standard value extrapolated from post-mortem measurement in erosion area [45]), temperature derived from IR data on "healthy" PFUs (next to the damaged one, such as PFU#8 see Fig. 13) are 450 °C and 520 °C for the "unshaped" and "shaped" geometries respectively. On the "damaged" PFUs, the surface temperatures reported in the middle of the MB are 450 $^{\circ}\text{C}$ (equivalent to the "healthy" PFU) and 750 °C (well above the "healthy" PFU) for type #2 and #3 damage respectively. Type #3 damage exhibits higher IR temperature with periodic modulation in the toroidal direction which is consistent with emissivity measurements showing the footprint of the ebeam grid pattern used during the HHF loading. The emissivity measured on the damaged area at room temperature ($\epsilon \sim 0.13$ reported on the peak of the periodic modulation, Fig. 13 left part of MB25) is

² The particle fluence is currently computed with flush Langmuir probes (LP) located in the lower divertor. Several issues were reported with the saturation current shape, in particular on the MB connected to the strike line. The values given in this paper are taken form the MB next to the one which is connected to the strike line where the saturation current exhibits standard profile. Reprocessing of the LP data could be considered in a near future.

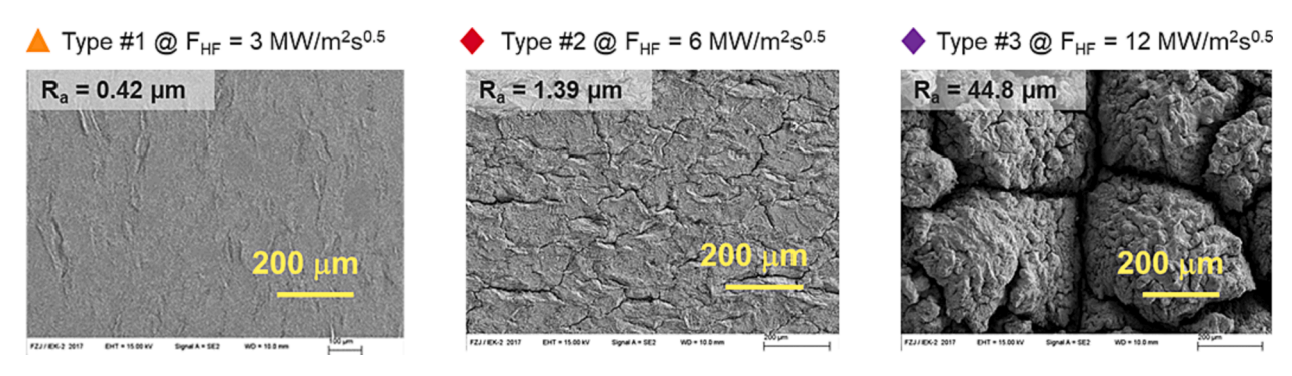


Fig. 10. (a) ELM-type damages generated with small, medium and large ELMs taken from [13].

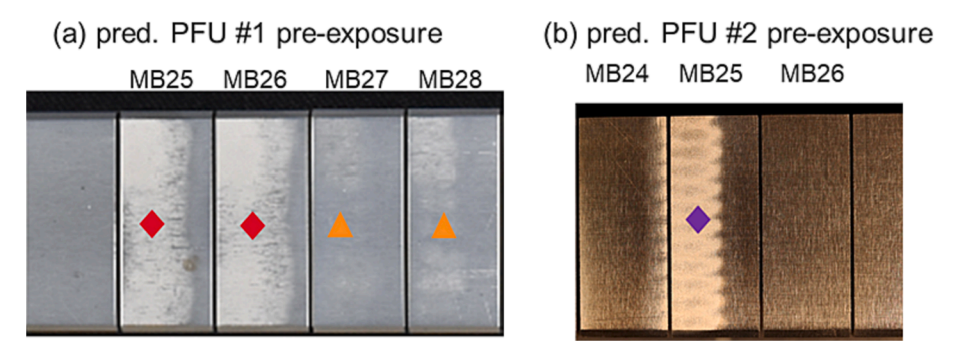


Fig. 11. PredPFU#1 exposed in WEST phase I (a) and PredPFU#2 exposed in phase II (b).

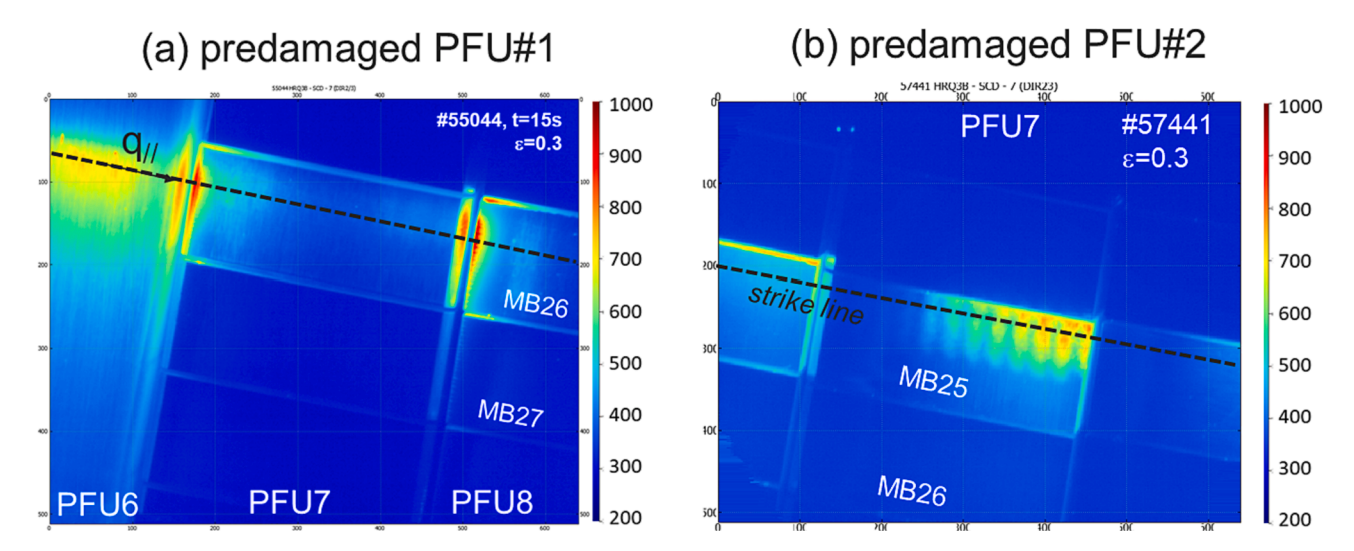


Fig. 12. IR measurement with the predamaged PFU#1 (crack network) and #2 (crack network and melted droplet) assuming surface emissivity $\epsilon = 0.3$.

about a factor of two higher than the one measured on healthy MBs ($\epsilon \sim 0.05$, Fig. 13 right part of MB25). Moving the outer strike line from MB25 to MB26 (12 mm away, in the low field side direction) and keeping the plasma parameters constant, it was also possible to compare the W-sources on "predamaged" MB (#25) with "healthy" MB (#26). No significant discrepancy was observed, suggesting that W sputtering is not affected by the surface morphology (roughness, cracks…).

To evaluate the evolution of the damage as function of plasma exposure time, Fig. 14 displays the toroidal temperature profiles measured at the beginning (blue) and at the end (red) of the high fluence experimental campaign. Using constant emissivity correction, the temperature profile exhibits periodic modulation consistent with the e-beam grid pattern used during the HHF loading as also observed with the emissivity measurement (dotted lines in Fig. 14-b). The surface

emissivity is found to decrease and sharply increase in the erosion and deposition areas, respectively. However, no noticeable differences are observed in-situ based on the IR data (full lines). The optical and material properties in the damaged area seems to be relatively robust regarding intensive and prolonged plasma exposures achieved in WEST. A detailed surface characterization is currently ongoing to evaluate the potential evolution of the cracks on the micrometer scale (length, width, and depth) as observed on predPFU#1. It is planned to reinstall PredPFU#2 in the machine for further plasma exposure in the next experimental campaigns (C8-C9).

6. Summary and prospects

A large number of ITER-grade PFUs and W blocks have been tested in

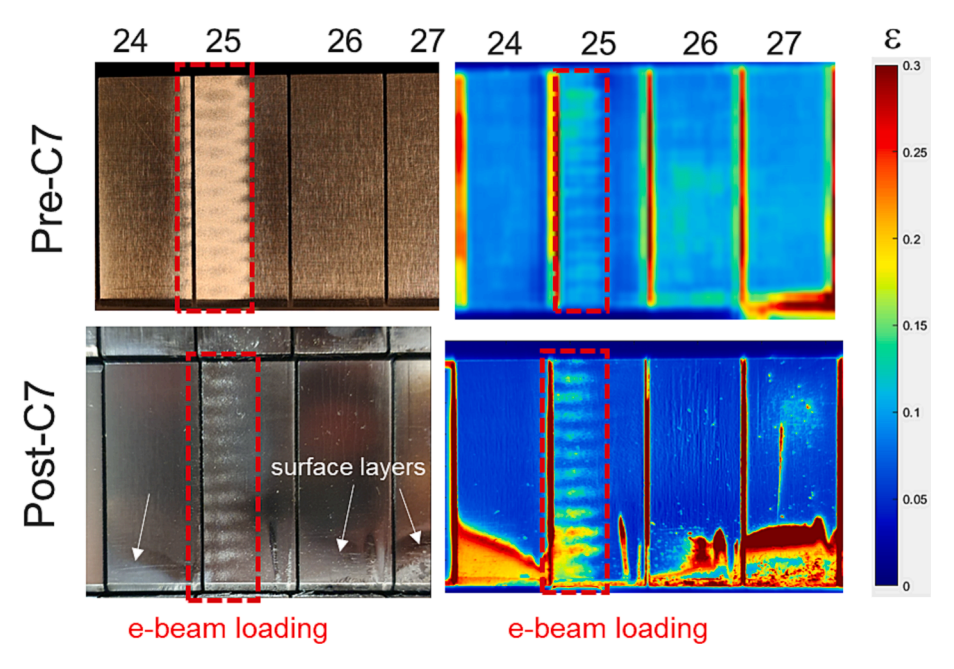


Fig. 13. Picture and emissivity measurements at room temperature on predPFU#2, before (top part) and after (bottom part) plasma exposure. The periodic modulation along the toroidal direction is due to the e-beam grid pattern.

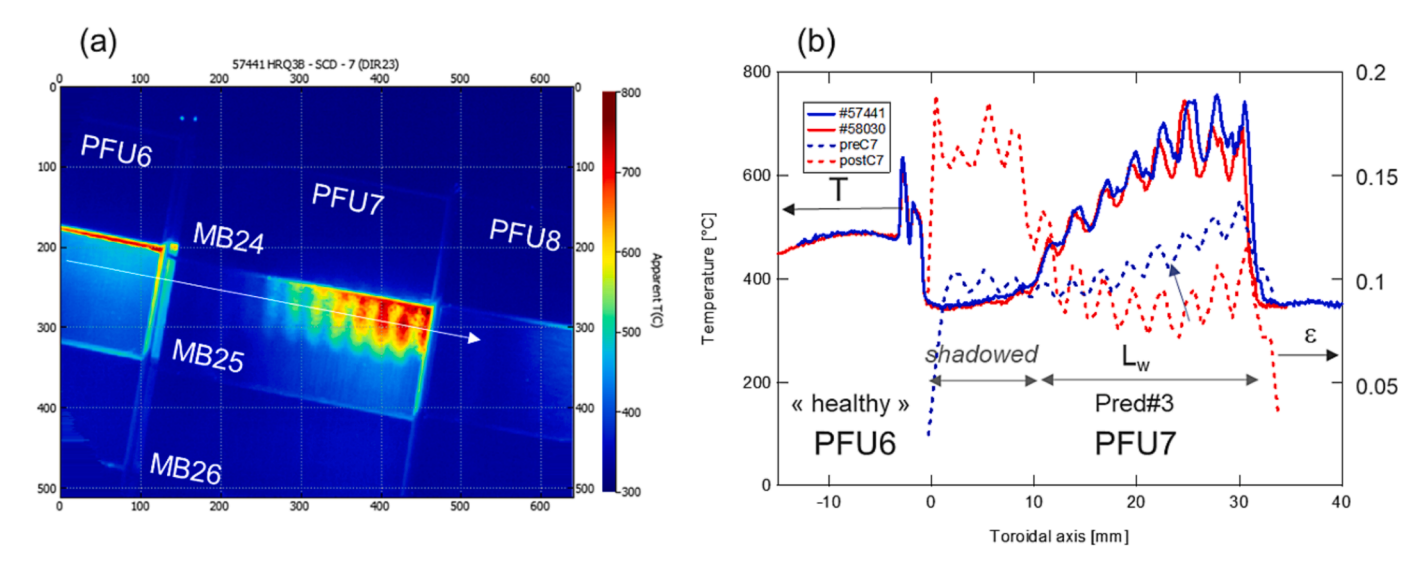


Fig. 14. (a) Apparent temperature map, with the VHR system looking at the pred#2 MB. (b) Full lines: temperature profile measured with the VHR IR system (assuming $\varepsilon = 0.3$ uniform) in the toroidal direction in the middle (blue) and the end (red) of the C6-C7 campaign. Dotted lines: emissivity profile measured before and after C6-C7 experimental campaign. (For interpretation of the references to colour in this figure legend, the reader is referred to the web version of this article.)

the WEST tokamak during phase I (C1-C5) and phase II first experimental campaigns (C6-C7). Several block geometries (shaped/unshaped), assembling configuration (vertical and radial misalignments) have been explored under various plasma condition (plasma heat load and position of the strike line). A very high spatial resolution (VHR) IR camera (0.1 mm/pixel) was used to derive the temperature and heat load distributions on the individual blocks during plasma experiments. IR data interpretation at the monoblock scale requires dedicated photonic modelling because of multifaceted and highly reflective thermal scene. Specular reflection is found to be dominant in toroidal gaps, trailing edges and chamfered surface. Optical hot spots predicted to occur in ITER due to plasma impact on PFU poloidal edges through toroidal gaps are not detected in-situ because they are located in the magnetically shadowed area (on a cold surface, not directly exposed to the plasma). With the heat load condition currently reach in WEST (≈ 6

 $\rm MW.m^{-2}$ deposited on the top surface of the block), the thermal signature of the OHS are below the IR detection threshold (typically 300 $^{\circ}\rm C$). Higher power on the top surface of the block would be required to bring the thermal signature of the OHS above the IR detection threshold.

Various W damage mechanisms have been identified as function of the heat loading exposure. For the misaligned/unshaped PFUs within the range of specified assembly tolerances (± 0.3 mm), regularly spaced cracking was observed on LEs. A dedicated modelling tool (TREX code) was developed to assess crack initiation under WEST conditions, showing that the observed crack pattern can be reproduced assuming brittle failure due to transients (600 MW.m $^{-2}$ for 3 ms disruption time).

Ductile failure has also been evidenced in WEST. For the first time, crack formation on the LE has been detected directly in the machine with the VHR IR system on a particular MB exposed to very high power load (2 kW power was deposited on one single block using the 2 mm

deep groove geometry). The VHR measurement gives a LE temperature of $\approx 2500~^\circ\text{C}$ for several seconds, outlining the impact of W recrystallization on the process. As predicted by modelling and experimental extrapolation, W-melting occurred under higher power loads (3 kW deposited power on the block). The observed melting onset and displacement were successfully modelled with the MEMENTO code. W-melting achieved in WEST under steady state heat load exhibits specific features: shallow melting, slow melt displacement, compared to transient melting observed in JET and AUG.

On the top surface of the unshaped blocks, post-mortem analysis did not show any evidence of cracking, except for one pre-damaged block featuring a micro-crack network pattern (created in a high heat flux facility before exposure in WEST), where broadening of the cracks and new cracks were observed after exposure in WEST [43]. Exposure of two pre-damaged PFUs have been performed at various levels: No significant degradation was observed so far (pending detailed based on ongoing post-mortem activities). A new PFU was recently taken out from the phase 2 fabrication batch and exposed to the JUDITH-2 e-beam to perform macrocrack (self-castellation) kind of damage [35] that might occur in tungsten after few cycles above 20 MW.m⁻². PredPFU#3 will be exposed in the next experimental campaign, together with predPFU#2 already exposed in WEST. In parallel to the plasma exposure and large scale testing of ITER grade PFUs foreseen in the future WEST experimental campaigns with the long discharge capabilities into action (the ultimate target being up to 1000 s), extensive post mortem analysis is pursued on phase 1 ITER-grade PFUs (flat top geometry) to characterize PFU damage, material migration, fuel retention and He-W plasma wall interaction.

CRediT authorship contribution statement

Y. Corre: Formal analysis. M-H. Aumeunier: Software, Visualization. A. Durif: Software, Visualization. J. Gaspar: Formal analysis, Visualization. K. Krieger: Conceptualization, Project administration. T. Loewenhoff: Formal analysis. M. Richou: Conceptualization, Supervision. S. Ratynskaia: Software, Visualization. Q. Tichit: Formal analysis, Visualization. Y. Anquetin: Formal analysis, Visualization. R. Dejarnac: Investigation. M. Diez: Formal analysis. L. Dubus: Investigation. M. Firdaouss: Software. J. Gerardin: Software, Visualization. A. Grosjean: Software, Visualization. J.P. Gunn: Formal analysis, Supervision. T. Loarer: Formal analysis, Supervision. P. Maget: Visualization. C. Martin: Formal analysis. K. Paschalidis: Software, Visualization. E. Tsitrone: Supervision, Project administration. M. Wirtz: Supervision, Project administration.

Declaration of Competing Interest

The authors declare that they have no known competing financial interests or personal relationships that could have appeared to influence the work reported in this paper.

Data availability

Data will be made available on request.

Acknowledgements:

"This work has been carried out within the framework of the EUROfusion Consortium, funded by the European Union via the Euratom Research and Training Programme (Grant Agreement No 101052200 — EUROfusion). Views and opinions expressed are however those of the author(s) only and do not necessarily reflect those of the European Union or the European Commission. Neither the European Union nor the European Commission can be held responsible for them."

References

- J. Bucalossi, et al., The WEST project: Testing ITER divertor high heat flux component technology in a steady state tokamak environment, Fusion Eng. Des. 89 (2014) 907–912.
- [2] T. Hirai, et al., Design optimization of the ITER tungsten divertor vectical targets, Fusion Eng. Des. 127 (2018) 66–72.
- [3] R.A. Pitts, et al., Physics basis for the first ITER tungsten divertor, Nuclear Materials and Energy 20 (2019), 100696.
- [4] J.P. Gunn, et al., Surface heat loads on ther ITER divertor vertical targets, Nucl. Fusion 57 (2017), 046025.
- [5] T. Hirai, et al., Use of tungsten material for the ITER divertor, Nuclear Material and Energy 9 (2016) 616–622.
- [6] M. Richou, Acceptance tests of the industrial series, Phys. Scr. 96 (2021), 124029.
- [7] M. Missirlian, et al., Manufacturing, testing and installation of the full tungsten actively cooled ITER-like divertor in the WEST tokamak, Fusion Eng. Des. 193 (2023), 113683.
- [8] G. Giruzzi, et al., Investigation of steady-state tokamak issues by long pulse experiments on Tore Supra, Nucl. Fusion 49 (2009), 104010.
- [9] M. Richou, et al., First plasma exposure of a pre-damaged ITER-like plasma-facing unit in the WEST tokamak: procedure for the PFU preparation and lessons learned, Nucl. Fusion 62 (2022), 056010.
- [10] R.A. Pitts, et al., Physics conclusions in support of ITER W divertor monoblock shaping, Nuclear Materials and Energy 12 (2017) 60–74.
- [11] A. Grosjean, et al., First analysis of the misaligned leading edges of ITER-like plasma facing units using a very high resolution infrared camera in WEST, Nucl. Fusion 60 (2020), 106020.
- [12] J.P. Gunn, et al., Thermal loads in gaps between ITER divertor monoblocks: First lessons learnt from WEST, Nuclear Materials and Energy 27 (2021), 100920.
- [13] A. Grosjean, et al., Very High Resolution Infrared imagery of misaligned tungsten monoblock edge heating in the WEST tokamak, Nuclear Materials and Energy 27 (2021), 100910.
- [14] J. Gaspar, et al., Divertor power loads and scrape off layer width in the large aspect ratio full tungsten tokamak WEST, Nucl. Fusion 61 (2021), 096027.
- [15] J. Bucalossi, et al., Operating a full tungsten actively cooled tokamak, Nucl. Fusion vol. 62 (2022), 042007.
- [16] M. Diez, et al., In situ observation of tungsten plasma-facing components after the first phase of operation of the WEST tokamak, Nucl. Fusion 61 (2021), 106011.
- [17] X. Courtois, et al., Full coverage infrared thermography diagnostic for WEST machine Protection, Fusion Eng. Des. 146 (2019) 2015–2202.
- [18] M. Houry, et al., The very high spatial resolution infrared thermography on ITER-like tungsten monobloks in WEST tokamak, Fusion Eng. Des. 146 (2019) 1104–1107.
- [19] J. Gaspar, et al., In situ assessment of the emissivity of tungten plasma facing components of the WEST tokamak, Nuclear Material and Energy 25 (2020), 100851.
- [20] Y. Corre, et al., Integration of fiber Bragg grating temperature sensors in plasma facing components of the WEST tokamak, Rev. Sci. Instrum. 89 (2018), 063508.
- [21] N. Chanet, et al., First temperature database achieved with Fiber Bragg Grating sensors in uncooled plasma facing components of the WEST lower divertor, Fusion Eng. Des. 170 (2021), 112528.
- [22] Y. Anquetin, et al., Surface heat flux estimation with embedded thermocouples and Fiber, Fusion Eng. Des. 190 (2023), 113480.
- [23] J. Gaspar, et al., Overview of the emissivity measurements performed in WEST: in situ and post-mortem observations, Nucl. Fusion 62 (2022), 096023.
- [24] N. Fedorczak, et al., Cross diagnostics measurements of heat load profiles on the lower tungsten divertor of WEST in L-mode experiments, Nuclear Materials and Energy 27 (2021), 100961.
- [25] M.-H. Aumeunier, et al., Infrared thermography in metallic environments of WEST and ASDEX upgrade, Nuclear Materials and Energy 26 (2021), 100879.
- [26] M. Firdaouss, et al., Heat flux depositions on the WEST divertor and first wall components, Fusion Eng. Des. 98 (2015) 1294.
- [27] A. Herrmann, Experiences with a solid tungsten divertor in ASDEX Upgrade, Nuclear Materials and Energy 12 (2017) 205–209.
- [28] G. Sergienko, et al., Experience with bulk tungsten test-limiters under high heat loads: melting and melt layer propagation, Phys. Scr. 81 (2007).
- [29] J. Coenen et al. ELM induced tungsten melting and its impact on tokamak operation Journal of Nuclear Materials 463 2015 78 8.
- [30] K. Krieger, et al., Experiments on transient melting of tungsten by ELMs in ASDEX Upgrade, Nucl. Fusion 58 (2) (2018), 026024.
- [31] J.W. Coenen, et al., Transient induced tungsten melting at the Joint European Torus (JET), Phys. Scr. 2017 (170) (2017), 014013.
- [32] J. Coenen, et al., Evolution of surface melt damage, its influence on plasma performance and prospects of recovery, J. Nucl. Mater. 463 (2013) 78.
- [33] G.Pautasso et al., "Details of power deposition in the thermal quench of ASDEX Upgrade disruptions," in 31st Conference on Plasma Physics, London, 28 June-2 July 2004
- [34] A. Durif, ., "t-rex., et al., Numerical tool for tungsten damage assessment for DEMO,", J. Nucl. Mater. 569 (2022), 153906.
- [35] A.Durif et al., "Cracks initiation and propagation of tungsten actively cooled ITER-like components during high power load experiment in WEST," in 19th International Conference on Plasma-Facing Materials and Components for Fusion Applications (PFMC), Bonn, 22 26 May, 2023.
- [36] Y. Corre, et al., Sustained W-melting experiments on actively cooled ITER-like plasma facing unit in WEST, Phys. Scr. 96 (2021), 124057.

- [37] Q. Tichit et al. Infrared detection of tungsten cracking on actively cooled ITER-like component during high power experiment in WEST in 19th International Conference on Plasma-Facing Materials and Components for Fusion Applications (PFMC) 22 May - 26 May 2023. Bonn.
- [38] K. Paschalidis et al. Melt dynamics with MEMENTO code development and numerical benchmarks in 19th International Conference on Plasma-Facing Materials and Components for Fusion Applications (PFMC) 2023 Bonn.
- [39] S. Ratynskaia, et al., Experiments and modelling on ASDEX Upgrade and WEST in support of tool development for tokamak reactor armour melting assessments, Nuclear Materials and Energy 33 (2022), 101303.
- [40] S. Ratynskaia, et al., Resolidification-controlled melt dynamics under fast transient tokamak plasma loads, Nucl. Fusion 60 (2020), 104001.
- [41] E. Thoren, et al., The MEMOS-U code description of macroscopic melt dynamics in fusion devices, Plasma Phys. Controlled Fusion 63 (2021), 035021.
- [42] T. Loewenhoff, et al., High pulse number thermal shock testing of tungsten alloys produced by powder injection molding, Nuclear Materials and Energy 20 (2019), 100680.

- [43] Y. Corre, et al., Plasma exposure of a pre-damaged ITER-like plasma facing unit in the WEST tokamak: in-situ and post-mortem measurements, Nuclear Materials and Energy 34 (2023), 101366.
- [44] M. Missirlian, et al., The WEST project: Current status of the ITER-like tungsten divertor, Fusion Eng. Des. 89 (7) (2014) 1048–1053.
- [45] J. Gaspar, et al., Emissivity measurement of the ITER-like plasma facing components of the WEST phase 2: Pre-exposure measurements and first WEST exposure, Nuclear Materials and Energy 33 (2022), 101305.

Further reading

- [46] S. Carpentier-Chouchana, Status of the ITER full-tungsten divertor shaping and heat load distribution analysis, Phys. Scr. (2014), 014002.
- [47] I. Z. e. al, Cracks avoidance with a modified solid tungsten divertor in ASDEX Upgrade, Fusion Eng. Des. 136 (2018) 1052–1057.